The Spatial Distribution of Ankle Muscles Activity Discriminates Aged from Young Subjects during Standing

Refined Structural Theories for the Random Response of Fiber-Reinforced and Sandwich Composite Structures

Matteo Filippi *, Marco Petrolo† and Erasmo Carrera ‡,
Politecnico di Torino, Turin, Italy, 10129

This paper presents numerical results concerning the structural dynamics of aerospace structures undergoing random excitations. The focus is on using refined structural models to investigate the accuracy of lower-order – Euler-Bernoulli and Timoshenko – and higher-order theories and, thus, determine the influence of some typical structural features, such as the shear deformation and warping. The numerical examples consider typical loadings with a random nature, white and jet noises, and gusts being common cases. The solution scheme is based on the finite element approach and the use of power and cross-spectral densities. The results are provided in the frequency domain using spectra and root mean square values of displacements and stresses. The results prove the ability of refined models to capture the dynamic responses at low and high frequencies. Moreover, as 1D models have superior computational efficiency compared to 2D and 3D ones, the proposed framework may have interesting perspectives in demanding analyses such as those concerning the fatigue life determination of complex aerospace structures.

I. Introduction

The prediction of the dynamic response of a structure subjected to random excitations is crucial to estimate the fatigue performance and, as a consequence, ensure a safe design. Gusts and noise excitations are only two examples of random loads that aircraft and space vehicles encounter during flights. According to a damage tolerance approach, stresses induced by these loads must be predicted to establish if (and when) a crack within a component will reach the critical size [1]. Stress and displacement histories can be calculated either by using the time signals of the random loads as inputs of dynamic analyses or by adopting the Power Spectral Density (PSD) concept. The latter procedure is preferred since computationally lighter than the direct integrations of the governing equation in the time domain. The structural response and loads are assumed to be stationary and ergodic stochastic processes in the PSD approach. Hence, their statistical parameters do not vary under time shifts and can be deduced through a single observation of the process itself over a long period.

The Finite Element (FE) Method has been extensively adopted to determine the spectra of displacements and stresses of structures. In most cases, the beam and plate/shell elements used for random analyses were based on classical and first-order shear deformation theories (see Refs. [2–5]). Although such elements are accurate enough for many structural configurations, the assumptions they rely on can be unacceptable for many other applications, such as laminated and thin-walled structures. The first option to overcome the limitations of classical 1D and 2D elements is using 3D (solid) formulations that can sometimes be unpracticable due to their computational cost. In this work, high-order finite beam elements are used to offer an accurate and computationally affordable alternative for predicting structural responses due to random excitations. These advanced one-dimensional theories are obtained using the Carrera Unified Formulation (CUF). Such a formalism enables finite element solutions based on arbitrary kinematic models to be generated with ease. The capabilities of 1D-CUF elements have been investigated by considering various problems, such as stress, dynamic, stability, and failure analyses of metallic, composite, and thin-walled structures (see Refs. [6–9]). Moreover, the formulation was revealed to be effective in solving multi-field problems (see Refs. [10, 11]). Systematic comparisons with two- and three-dimensional finite element solutions demonstrated that 1D-CUF models provide 3D-like solutions requiring, generally, a lower computational cost.

*Assistant Professor, Department of Mechanical and Aerospace Engineering, matteo.filippi@polito.it
†Associate Professor, Department of Mechanical and Aerospace Engineering, marco.petrolo@polito.it
‡Full Professor, Department of Mechanical and Aerospace Engineering, erasmo.carrera@polito.it

II. Theoretical section

A. Proposed analysis

The power spectral densities of the three-dimensional displacement (S_u) and the stress (S_σ) components at various frequencies (ω) are correlated with the PSD of the load (S_F) by the following equation

$$\begin{aligned} S_{u_i}(\omega) &= \bar{H}_{u_i}(\omega)\, S_F(\omega)\, H^T{}_{u_i}(\omega) \qquad i = 1,2,3 \\ S_{\sigma_j}(\omega) &= \bar{H}_{\sigma_j}(\omega)\, S_F(\omega)\, H^T{}_{\sigma_j}(\omega) \qquad j = 1,\ldots,6 \end{aligned} \tag{1}$$

$\bar{H}(\omega)$ and $\bar{H}^T(\omega)$ are, respectively, the complex conjugate and the transpose of the admittance matrix $\bar{H}(\omega)$. Admittance matrices can be computed with the Finite Element (FE) method by performing as many frequency response analyses as of the non-null terms (nnz) in the generalized force vector (F). For an arbitrary non-null generalized coordinate (k), the matrix is

$$H_{q_k}(\omega) = [q_{k1}\, q_{k2}\, \ldots,\, q_{kL}] \qquad k = 1,\ldots,nnz \qquad L = 1,\ldots,fs \tag{2}$$

where fs is the number of frequency steps. The column vector (q) collects the Degrees of Freedom (DoF) of the FE model and it is derived from the following equation

$$q_k(\omega) = [-\omega^2 M + i\omega C + K]^{-1} F_k^* \qquad i = \sqrt{-1} \tag{3}$$

The vector F_k^* has only one non-null term (equal to 1). Its position corresponds to that of the k non-null term of the vector F. The terms M, C, and K are the mass, damping, and stiffness matrices of the FE model. For reducing the computational burden, it is customary to adopt the modal reduction strategy that makes use of an arbitrary number (nm) of eigenvectors (x_j) determined from the undamped, homogeneous equation of motion

$$[-\omega_j^2 M + K] x_j e^{i\omega_j t} = 0 \qquad j = 1,\ldots,nm \tag{4}$$

By collecting the eigevectors in a $DoF \times nm$ matrix (X), Eq. (3) becomes

$$X^T q_k(\omega) = [-\omega^2 (X^T M X) + i\omega (X^T C X) + (X^T K X)]^{-1} X^T F_k^* \qquad i = \sqrt{-1} \tag{5}$$

B. The advanced finite beam elements

The accuracy and the computational time required by the analyses depend on the dimensionality of the FE model and the kinematic assumptions adopted to approximate the primary variables. Beam and plate/shell formulations based on low-order shear deformation models enable accurate results to be obtained for structures with well-defined material anisotropy's degree and geometrical characteristics. Moreover, these theories can provide inaccurate distributions of derivative quantities, namely the strain and stress fields. To extend the range of applicability of 1D and 2D FE models, one strategy is to enrich the kinematic expansions in an axiomatic fashion. The Carrera Unified Formulation allows one to derive low- and high-fidelity finite elements with ease by exploiting a simple indicial notation. For one-dimensional models, the formulation is

$$u(x,y,z,t) = F_\tau(x,z) N_i(y) u_{\tau i}(t) \qquad \tau = 1,\ldots,M \quad i = 1,\ldots,sn \tag{6}$$

where $F_\tau(x,z)$ are arbitrary functions defined above the beam's cross-section, $N_i(y)$ are the FE shape functions along the beam's axis, M is the number of terms included in the expansion, and sn is the number of structural nodes for each beam element. The repeated subscripts indicate summation. It should be highlighted that the number and the type of the $F_\tau(x,z)$ functions are input parameters of the analysis; therefore, it is possible to derive, at least theoretically, an infinite number of kinematic fields. In this work, two polynomial bases are adopted to approximate the kinematic field: the Taylor and Lagrange expansion classes (denoted as TE and LE). A generic K-order TE model (TEK) includes $M=\frac{(K+1)(K+2)}{2}$ power functions of the cross-section's coordinates. The second-order TE model (TE2), for example, is

$$\begin{aligned} u_x &= u_{x_1} + x\, u_{x_2} + z\, u_{x_3} + x^2\, u_{x_4} + xz\, u_{x_5} + z^2\, u_{x_6} \\ u_y &= u_{y_1} + x\, u_{y_2} + z\, u_{y_3} + x^2\, u_{y_4} + xz\, u_{y_5} + z^2\, u_{y_6} \\ u_z &= u_{z_1} + x\, u_{z_2} + z\, u_{z_3} + x^2\, u_{z_4} + xz\, u_{z_5} + z^2\, u_{z_6} \end{aligned} \tag{7}$$

The refined expansion of Eq. 7 has 18 generalized displacement variables: three constant, six linear, and nine parabolic terms. The classical beam theories can be derived as particular cases of the first order Taylor-like expansion (TE1). To obtain the first-order shear deformation theory (FSDT), the linear terms, u_{x_2}, u_{x_3}, u_{z_2}, u_{z_3} can be neglected, and the elastic rotations θ_z and ϕ_x are assumed equal to u_{y_2} and u_{y_3}. When the LE approach is utilized, the section is divided into a number of subdomains on which two-dimensional Lagrange functions are defined. The LE polynomial degree is determined by the number of nodes used to delimit each subdomain. Bi-linear, bi-quadratic, and bi-cubic Lagrange functions are obtained with four (LE4), nine (LE9), and sixteen (LE16) nodes, respectively. The number of terms included in the kinematic field, M, is the total number of nodes belonging to the cross-section. For more details, the interested reader may refer to Ref. [12].

The use of Eq. 6 into a variational principle allows one to derive FE matrices and vectors by adequately assembling the so-called *Fundamental Nuclei*, namely 3-by-3 matrices or 3-by-1 vectors. Their components do not depend on both the number and type of functions utilized in the kinematic expansions. For the sake of clarity, the derivation of *Fundamental Nuclei* for the stiffness matrix and the force vector is below reported. According to the Principle of Virtual Displacement (PVD), the virtual variation of the strain energy δL_{int} equals the virtual variation of the work done by external loads δL_{ext}

$$\delta L_{int} = \delta L_{ext} \tag{8}$$

The virtual variation of the internal work can be written as:

$$\delta L_{int} = \delta \mathrm{u}^{\mathrm{T}}{}_{sj} \int_V \left[N_j(y) F_s(x,z)\ \mathrm{D}^{\mathrm{T}}\ \bar{\mathrm{C}}\ \mathrm{D}\ F_\tau(x,z) N_i(y) \right] dV\ \mathrm{u}_{\tau i} = \delta \mathrm{u}^{\mathrm{T}}{}_{sj}\ \mathrm{K}^{ij\tau s}\ \mathrm{u}_{\tau i} \tag{9}$$

where V is the body volume while D and $\bar{\mathrm{C}}$ are, respectively, a differential operator and the matrix of the elastic coefficients of the linear geometrical and constitutive relations. Subscripts s and j are utilized for the virtual variation of displacements and they have the same meanings and bounds of indexes τ and i of Eq. 6. The matrix $\mathrm{K}^{ij\tau s}$ is the *fundamental nucleus* of the stiffness matrix. On the other hand, the work done by volume F_V, surface F_A, and point F_P forces can be written as

$$\delta L_{ext} = \int_V \delta \mathrm{u}^{\mathrm{T}} \mathrm{F}_V\ dV + \int_A \delta \mathrm{u}^{\mathrm{T}}{}_A \mathrm{F}_A\ dA + \delta \mathrm{u}^{\mathrm{T}}{}_P \mathrm{F}_P \tag{10}$$

The cross-spectral density matrix $\mathrm{S_F}$ is derived from the expressions of the generalized forces in Eq. 10.

C. The cross-spectral density matrix for a pressure

The generalized nodal force vector for a pressure F_A exerted on a surface A defined by the coordinates χ (or ζ) and y at instant t can be expressed as

$$\mathrm{F}(t) = \int_A F_s(\chi,\zeta) N_j(y) \mathrm{F}_A(\chi(\zeta), y, t)\ dA \tag{11}$$

The correlation matrix for the generalized nodal forces between two instants is

$$\mathrm{R_F}(t_1,t_2) = \int_A F_s(\chi,\zeta) N_j(y)\ \int_A F_s(\chi,\zeta) N_j(y) E[\mathrm{F_A}(\chi_1(\zeta_1),\zeta,t_1)\mathrm{F_A}(\chi_2(\zeta_2),\zeta,t_2)] dA\, dA \tag{12}$$

Since the pressure spectrum is assumed to be stationary, the correlation function only depends on the time shift (t_2-t_1); therefore, by taking the Fourier transform of Eq. 12, the cross-spectral density matrix of generalized nodal forces becomes

$$\mathrm{S_F}(\omega) = \int_{Al} F_s(\chi,\zeta) N_j(y)\ \int_{Am} F_s(\chi,\zeta) N_j(y) \mathrm{S_P}(\omega) dAm\, dAl \tag{13}$$

in which $\mathrm{S_P}(\omega)$ is the pressure cross-spectral densisty matrix. According to Ref. [4], Eq. 13 is simplified as

$$\mathrm{S_F}(\omega) = \int_A F_s(\chi,\zeta) N_j(y) dA\ (\mathrm{S_P}(\omega))\ \int_A F_s(\chi,\zeta) N_j(y) dA \tag{14}$$

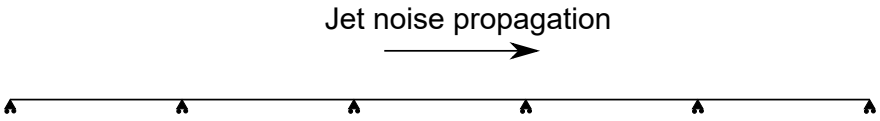

Fig. 1 The five-span beam subjected to jet noise.

III. Numerical results

The first application concerned the response of the five-span beam shown in Fig. 1.
Each bay was 1 meter long with a transverse area of 0.01x0.01 m^2. Young modulus and density were equal to 1.2 GPa and 10000 kgm^{-3}, respectively. The beam was subjected to an acoustic noise, which propagates along its span. This simple model represents the panel-rib-stringer assembly of aircraft structures subjected to a pressure field induced downstream by jet engine exhausts. The CSD matrix of the pressure is

$$S_P(\omega) = exp\left(-\frac{i\,\omega\,\bar{y}}{C_0\,L}\right) \tag{15}$$

where C_0 is the nondimensional propagation velocity of the wave (equal to 6), L is the length of the beam (5 m) and $(\bar{y})$ is the distance between two points along the beam span. Table 1 lists the first ten natural frequencies calculated with four 1D-CUF models. The two finite element models utilized for discretizing the structure along the longitudinal axis consisted of ten and twenty 3-node beam elements (*B3*). The adopted structural theories were the first-order shear deformation theory (FSDT) and the bi-cubic Lagrange-type expansion (1-LE9). The comparisons with the solution presented in Ref. [5] revealed that, at least, twenty beam elements are required to detected accurately the first ten mode shapes, regardless of which structural theories are used.

Table 1 Natural frequencies (in Hz) of the five-bay beam.

Mode	FSDT/10B3	FSDT/20B3	1-LE9/10B3	1-LE9/20B3	Ref. [5]
1	1.5885	1.5718	1.5885	1.5718	1.5708
2	1.7671	1.7440	1.7671	1.7440	1.7427
3	2.2285	2.1819	2.2285	2.1819	2.1793
4	2.8481	2.7505	2.8481	2.7505	2.7449
5	3.4876	3.3054	3.4876	3.3054	3.3047
6	6.9698	6.3516	6.9698	6.3516	6.2831
7	7.5407	6.7231	7.5407	6.7231	6.6417
8	8.9135	7.5817	8.9135	7.5817	7.4648
9	10.765	8.6271	10.765	8.6271	8.4549
10	12.800	9.6196	12.800	9.6195	9.3800

Figure 2-(a) shows the power spectral density computed with the selected theories at y = 0.5 m. The reduced-order models were developed by retaining 20 mode shapes and assuming a modal damping ratio equal to 1% of the critical value.
For the first band of frequencies (up to 6 Hz), the 1D-CUF theories provided similar results while the discrepancies between the PSD peaks become appreciatable for larger frequency values. Table 2 reports the root mean square (RMS) displacements at various locations calculated with the 1D-CUF models and those obtained with other finite element formulations presented in Refs. [2**?**]. Comparisons revealed that the first-order shear deformation theory provided higher RMS values than those obtained with the other approaches. However, it should be underlined that the RMS values were computed by integrating the PSD functions for a given frequency range; therefore, these values can be affected by the accuracy of the used integration method. Figure 2-(b) illustrates the power spectral density of the vertical displacements at two equidistant positions from the beam ends. The curves are not overlapped since the jet noise was idealized as a moving wave from left to right of the structure.
The following section reports the results in terms of PSD and RMS for the simply-supported beam shown in Fig. 3, which was excited by a clipped white noise with cut-off frequency ω_c = 85 rad sec^{-1}. Its geometrical and material

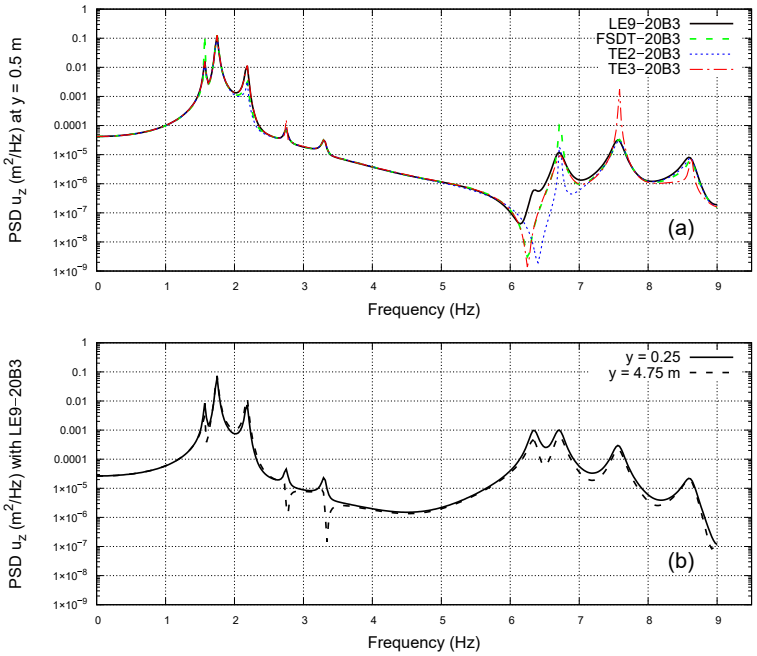

Fig. 2 Power spectral densities for the five-span beam (a) computed with various theories, and (b) at different positions.

Table 2 Root mean square displacements.

Location [m]	FSDT	1-LE9	Ref. [2]	Ref. [**?**]
0.25	0.2073	0.1824	0.1718	0.1820
0.50	0.2639	0.2376	0.2273	0.2349
0.75	0.1963	0.1660	0.1557	0.1656
4.25	0.1977	0.1675	0.1792	0.1670
4.50	0.2754	0.2501	0.2390	0.2478
4.75	0.2133	0.1888	0.1792	0.1884

properties are listed in Tab. 3.

Table 3 The simply-supported beam.

Geometrical data	**Material data**
$L = 1.0$ m	Young modulus (E) = 0.12 GPa
$h = 10^{-2}$ m^2	Poisson's ratio (ν) = 0.0
$b = 10^{-1}$ m^2	Density (ρ) = 10^3 kgm^{-3}

The mathematical model consisted of ten cubic beam elements corresponding to 31 structural nodes. The random load was idealized with a set of 31 concentrated vertical forces, each of them applied at one structural node of the FE model. The resultant force was 1 N. The damping matrix was defined as C = g K + d M with $g = 0.01$ and $d = 0$. Figure 4 shows the power spectral densities of the vertical displacement u_z at (0, $L/2$, 0), the axial stress $\sigma_{\rm yy}$ at (0, $L/4$, $-h/2$) and the transverse shear stress $\sigma_{\rm yz}$ at (0, $L/4$, 0) calculated with the first-order shear deformation theory, the quadratic models (TE2 and 1-LE9), and the cubic expansion (TE3).
The models provided the same PSDs for u_z and σ_{yy}. Instead, the power spectral density of σ_{yz} calculated with the cubic model differs significantly from the others. The TE3 model foresees a quadratic through-the thickness distribution of

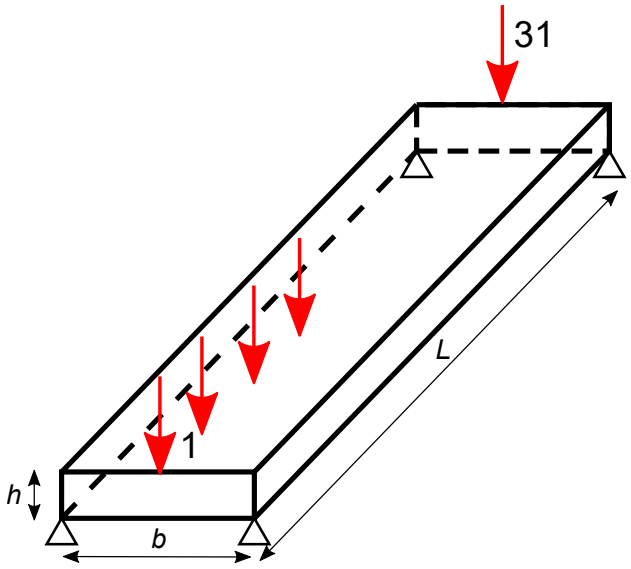

Fig. 3 The simply-supported beam subjected to a white noise.

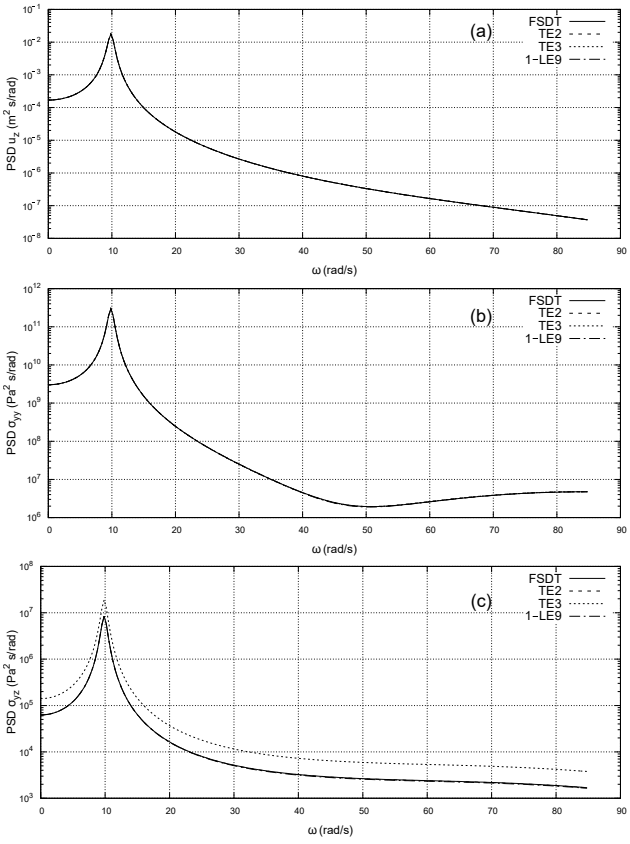

Fig. 4 Power spectral densities of the (a) vertical displacement, (b) normal and (c) shear stresses.

the transverse shear stress, while the FSDT and the quadratic theories provide constant and linear profiles, respectively. Such variations are illustrated in Fig. 5, where the root mean squares of the transverse shear stress are shown along the beam's thickness.

It is possible to observe that the maximum σ_{yz} value obtained with the TE3 theory is 50% larger than those calculated

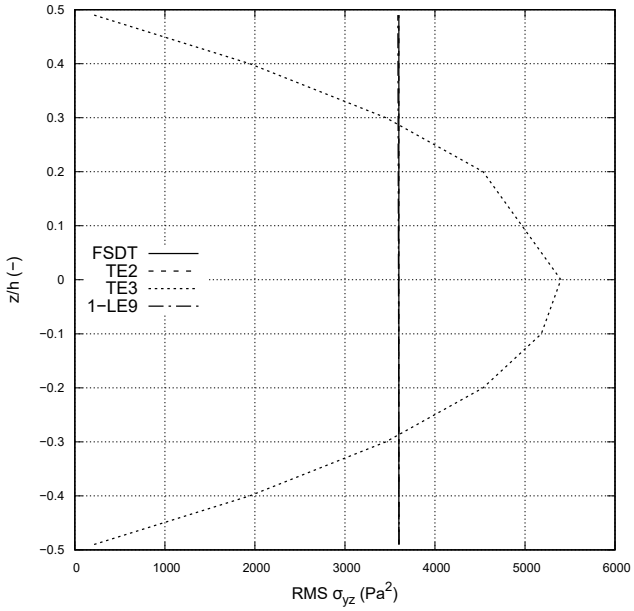

Fig. 5 Root mean square of the transverse shear stress along the thickness at one-quarter of the span.

with the other models. Because the fatigue analyses require the spectra of stress components at many structure points as inputs (see Ref. [13]), the use of inaccurate stress descriptions may be questionable, especially for composite and sandwich structures.

Next, the response of the laminated box beam shown in Fig. 6 and subjected to uniformly distributed atmospheric turbulence was studied. The dimensions of the structure and material properties are reported in Tab. 4.

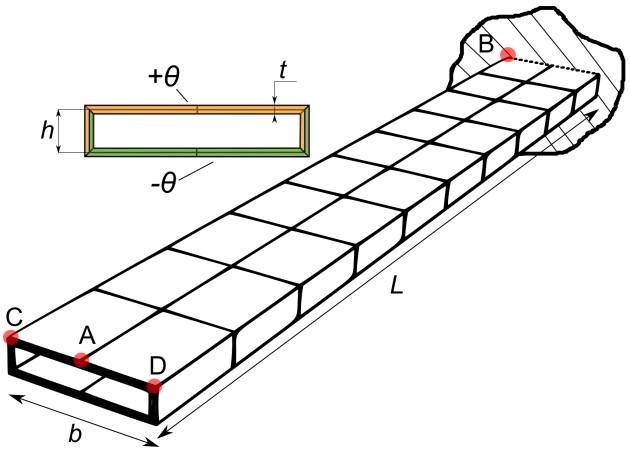

Fig. 6 The box beam and the lamination scheme of the cross-section.

Table 4 The laminated box beam of Fig. 6.

Geometrical data	Material data
L = 2.032 m	E_1 = 206.92 GPa $E_{2,3}$ = 5.17 GPa
h = 0.0508 m	$G_{13,23}$ = 2.55 GPa G_{12} = 3.10 GPa
b = 0.254 m	$\nu_{12,13,23}$ = 0.25
t = 0.01016 m	ρ = 1529.48 kgm^{-3}

The von Kármán spectrum was adopted to model the atmospheric gust

$$S_P = \frac{L_s}{\pi V_s} \frac{1 + (8/3)[1.339(L_s/V_s)\omega]^2}{(1 + [1.339(L_s/V_s)\omega]^2)^{11/6}}$$

L_s and V_s are, respectively, the scale length of the turbulence and the airspeed. The structure was again discretized with ten cubic beam elements, and the viscous damping was assumed equal to 0.5% of the critical value. The responses were obtained by retaining 30 eigenvectors in the reduced-order models. Figures 7-(a) and -(b) report the power spectral densities of the vertical displacement and the axial stress, σ_{yy}. The Lagrange-type solution (12-LE9) was developed utilizing twelve nine-node elements: two elements for each lateral edge and four for the top and bottom surfaces.

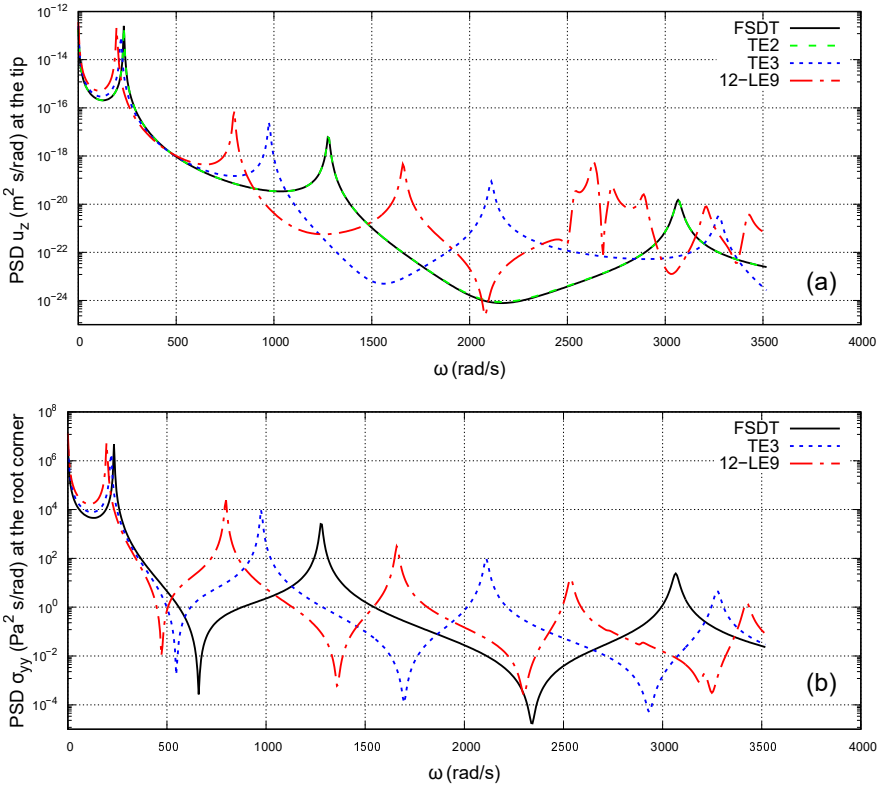

Fig. 7 Power spectral densities of vertical displacement of Point A and axial stress of Point B for the laminated box beam (see Fig. 6). θ **= 0** deg**.**

For this structure, significant discrepancies between the results can also be observed in the vertical displacement PSDs. The structural response is indeed strongly affected by local deformations of the thin-walled cross-section, which are captured accurately only by the LE solution. However, rising the order of the Taylor expansion, the TE solutions converge to the LE result. Figures 8-(a) and -(b) show, respectively, the power spectral densities of vertical and axial displacements of Points C and D (see Fig. 6) for θ = 30 deg. The differences between the curves of the two points are due to the adopted lamination scheme, which leads to circumferentially asymmetric stiffness configurations. For this reason, the structure deformations exhibit flexural-torsional couplings when θ is not equal to either 0 or 90 deg.
Eventually, the response of a sandwich cantilever beam subjected to four-point loads (1 N) was studied (see Fig. 9). Table 5 lists the dimensions and material properties of the soft-core (denoted with the subscript 'c') and the metallic faces (indicated with the subscript 'f'). Seven four-node beam elements were utilized along the longitudinal axis while the displacement variables on the cross-section were approximated with the TE2, TE3, TE6, and 3-LE16 models. The modal damping was 1% of the critical value.
Figures 10-(a) and (b) graphically illustrate the PSDs of vertical displacement and axial stress calculated with the selected theories. It can be observed that the peak corresponding to the first bending mode shape occurs at lower frequencies as the model kinematics is enriched. The differences between the results are due to the deformability of the soft-core that significantly affects the structural response. Although the TE2 model improves the first-order shear

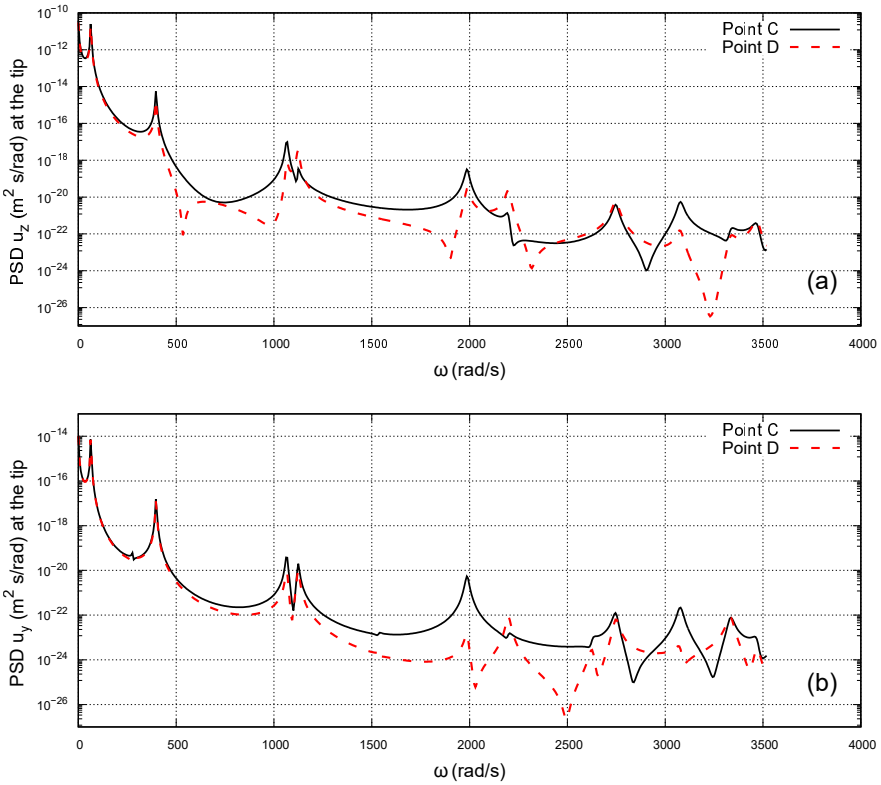

Fig. 8 Power spectral densities of displacements of Points C and B calculated with the 12-LE9 solution. θ **= 30** deg**.**

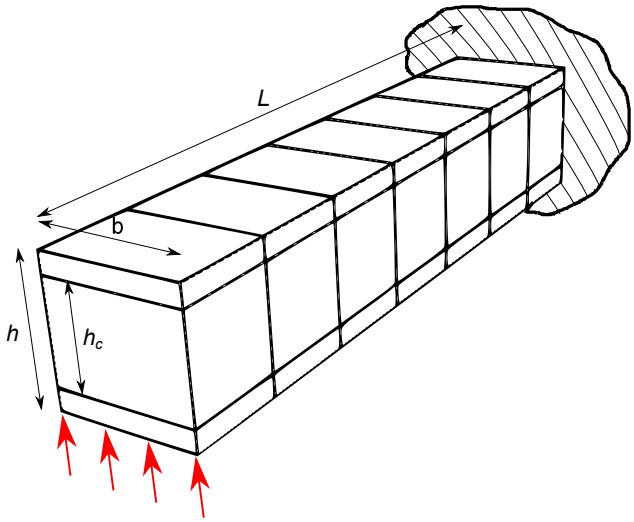

Fig. 9 The sandwich beam and the loading condition.

deformation theory, it overestimates to a remarkable extent the bending frequency. Indeed, no peaks appear within the considered frequency interval. The root mean squares of σ_{yy} and σ_{yz} for various thickness coordinates are illustrated in Figs. 11-(a) and -(b), respectively. As far the axial stress is concerned, it is possible to observe that the Lagrange-type solution provided an asymmetric profile with respect to the mean axis. The LE model predicted the maximum value within the core for the transverse shear stress, whereas the TE2 expansion erroneously provided the maximum values at the top and bottom surfaces.

Table 5 Material and geometrical properties of the sandwich beam shown in Fig. 9.

Geometrical data	Material data
$L = 0.1$ m	$E_f = 200.0$ GPa $E_c = 0.66$ GPa
$h = b = 0.02$ m	$\nu_f = 0.27$ $\nu_c = 0.3$
$h_c = 0.014$ m	$\rho_f = 7800$ kgm^{-3} $\rho_c = 60.0$ kgm^{-3}

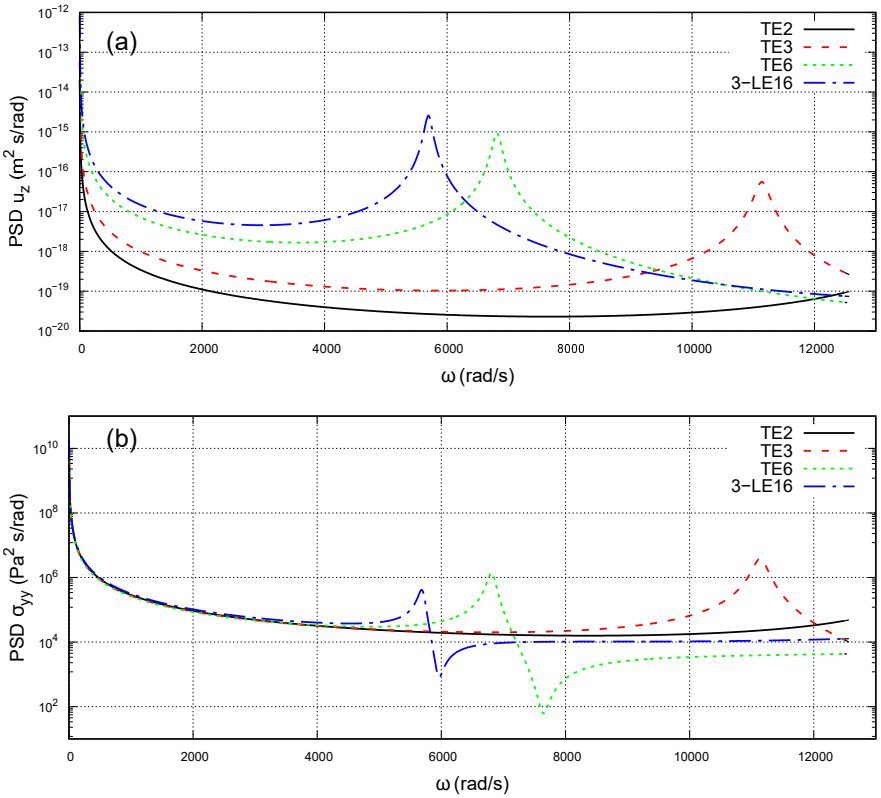

Fig. 10 Power spectral densities of the (a) vertical displacement and (b) axial normal stress, σ_{yy}, computed at (b/2, L/2, h/2).

IV. Conclusions

This paper explored the capabilities of advanced finite beam elements to predict dynamic responses of structures subjected to random excitations. The one-dimensional models were developed by exploiting a unified formulation that enables low and high-fidelity solutions to be easily obtained. Results were reported in terms of power spectral densities and root mean square values of displacement and stress components. The numerical applications concerned two typical beam-like structures, a laminated thin-walled beam, and a sandwich configuration. The differences between results provided by low-order models and those calculated with advanced theories were remarkable in some cases, especially for the stress components. Because fatigue performance predictions require accurate evaluations of the stress field, precise and computationally light finite element solutions could be a viable and advantageous alternative to the two- and three-dimensional finite element models.

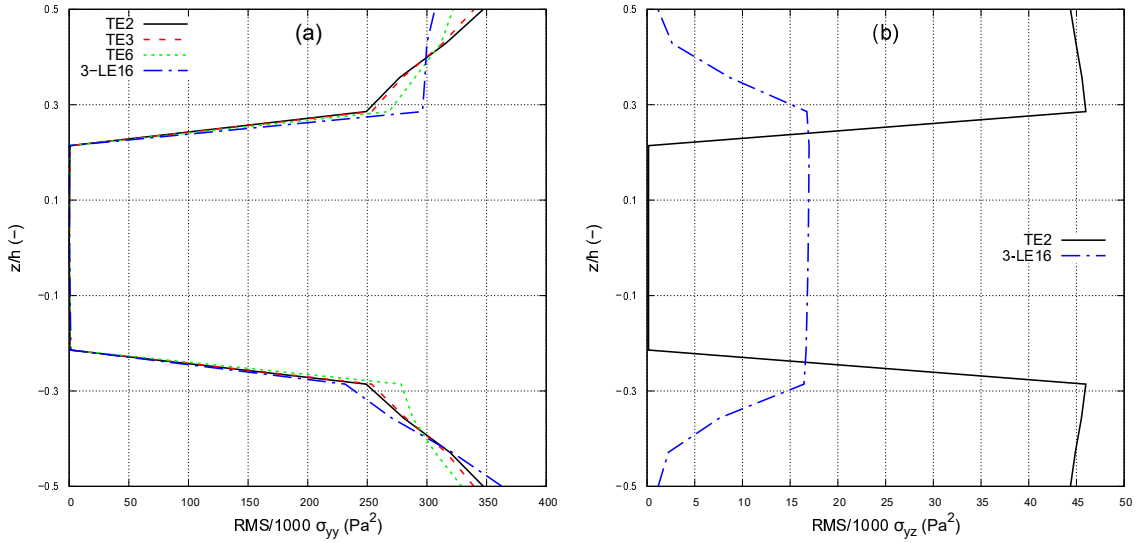

Fig. 11 Root mean square of the (a) axial stress and (b) transverse shear stress through-the-thickness at (*b*/2, *L*/2, z).

References

[1] Halfpenny, A., "A frequency domain approach for fatigue life estimation from finite element analysis," *Key Engineering Materials*, Vol. 167, 1999, pp. 401–410.

[2] Olson, M. D., "A consistent finite element method for random response problems," *Computers & Structures*, Vol. 2, No. 1-2, 1972, pp. 163–180.

[3] Dey, S. S., "Finite element method for random response of structures due to stochastic excitation," *Computer Methods in Applied Mechanics and Engineering*, Vol. 20, No. 2, 1979, pp. 173–194.

[4] Goswami, S., "Response of composite stiffened shells under stochastic excitation," *Journal of reinforced plastics and composites*, Vol. 16, No. 16, 1997, pp. 1492–1522.

[5] Liu, Q., Orisamolu, I., and Chernuka, M., "Consistent finite element discretization of distributed random loads," *Computers & structures*, Vol. 51, No. 1, 1994, pp. 39–45.

[6] Carrera, E., and Petrolo, M., "Refined one-dimensional formulations for laminated structure analysis," *AIAA journal*, Vol. 50, No. 1, 2012, pp. 176–189.

[7] Carrera, E., Pagani, A., and Petrolo, M., "Classical, refined, and component-wise analysis of reinforced-shell wing structures," *AIAA journal*, Vol. 51, No. 5, 2013, pp. 1255–1268.

[8] Kaleel, I., Petrolo, M., Waas, A., and Carrera, E., "Micromechanical progressive failure analysis of fiber-reinforced composite using refined beam models," *Journal of Applied Mechanics*, Vol. 85, No. 2, 2018.

[9] Wu, B., Pagani, A., Filippi, M., Chen, W., and Carrera, E., "Large-deflection and post-buckling analyses of isotropic rectangular plates by Carrera Unified Formulation," *International Journal of Non-Linear Mechanics*, Vol. 116, 2019, pp. 18–31.

[10] Entezari, A., Filippi, M., and Carrera, E., "Unified finite element approach for generalized coupled thermoelastic analysis of 3D beam-type structures, part 1: Equations and formulation," *Journal of Thermal Stresses*, Vol. 40, No. 11, 2017, pp. 1386–1401.

[11] Filippi, M., Entezari, A., and Carrera, E., "Unified finite element approach for generalized coupled thermoelastic analysis of 3D beam-type structures, part 2: Numerical evaluations," *Journal of Thermal Stresses*, Vol. 40, No. 11, 2017, pp. 1402–1416.

[12] Carrera, E., Cinefra, M., Petrolo, M., and Zappino, E., *Finite element analysis of structures through unified formulation*, John Wiley & Sons, 2014.

[13] Reytier, T., Bes, C., Marechal, P., Marco, B., and Santgerma, A., "Generation of correlated stress time histories from continuous turbulencePower Spectral Density for fatigue analysis of aircraft structures," *International Journal of Fatigue*, , No. 42, 2012, pp. 147–152. https://doi.org/10.1016/j.ijfatigue.2011.08.013.